

# PCCP

Accepted Manuscript



This is an *Accepted Manuscript*, which has been through the Royal Society of Chemistry peer review process and has been accepted for publication.

*Accepted Manuscripts* are published online shortly after acceptance, before technical editing, formatting and proof reading. Using this free service, authors can make their results available to the community, in citable form, before we publish the edited article. We will replace this *Accepted Manuscript* with the edited and formatted *Advance Article* as soon as it is available.

You can find more information about *Accepted Manuscripts* in the [Information for Authors](#).

Please note that technical editing may introduce minor changes to the text and/or graphics, which may alter content. The journal's standard [Terms & Conditions](#) and the [Ethical guidelines](#) still apply. In no event shall the Royal Society of Chemistry be held responsible for any errors or omissions in this *Accepted Manuscript* or any consequences arising from the use of any information it contains.

## Biofuel purification in zeolitic imidazolate frameworks: significant role of functional groups

Kang Zhang, Anjaiah Nalaparaju, Yifei Chen<sup>†</sup>, and Jianwen Jiang\*

*Department of Chemical and Biomolecular Engineering, National University of Singapore, 117576, Singapore*

A molecular simulation study is reported for biofuel purification in six zeolitic imidazolate frameworks (ZIF-8, -25, -71, -90, -96 and -97) with different functional groups. For pure ethanol and water, the predicted adsorption isotherms agree fairly well with experimental data. Hydrogen bonding has an important effect on the adsorption of ethanol and water. In hydrophilic ZIFs (ZIF-90, -96 and -97) with polar groups, adsorption capacities are higher than in hydrophobic counterparts (ZIF-8, -25 and -71). The atomic charges in symmetrically functionalized ZIF-8, -25, and -71 are found to have indiscernible effect on adsorption, in remarkable contrast to asymmetrically functionalized ZIF-90, -96 and -97. For ethanol/water mixtures representing biofuel, the selectivity of ethanol/water drops with increasing ethanol in mixtures. It is revealed that the selectivity is determined primarily by framework hydrophobicity as well as cage size. Among the six ZIFs, ZIF-8 exhibits the highest selectivity. This simulation study provides microscopic insight into the adsorption of ethanol and water in various ZIFs, reveals the significant role of functional groups in governing biofuel purification, and would facilitate the development of new nanoporous materials for high-efficacy liquid separation.

\*E-mail: chejj@nus.edu.sg

<sup>†</sup>Current address: Tianjin University-SINOPEC R & D Center for Petrochemical Technology, Tianjin University, Tianjin, 300072, China

**Electronic supplementary information (ESI) available:**

Pores, fragmental clusters, atomic charges, potential parameters of ZIFs, EtOH and H<sub>2</sub>O; accessibility in ZIF-96 and ZIF-97; adsorption isotherms of EtOH with and without atomic charges; vapor-liquid equilibria and fugacities of EtOH/H<sub>2</sub>O mixtures; adsorption isotherms of EtOH/H<sub>2</sub>O mixtures.

## 1. Introduction

With increasing demand for energy and growing level of greenhouse gas in the atmosphere, there has been considerable interest in biofuel as alternative renewable energy resource.<sup>1,2</sup> In contrast to fossil fuel, biofuel is environmentally benign and carbon neutral with less emission of gaseous pollutants. Produced from biological feedstock (e.g. algae, miscanthus, corn, etc.), biofuel contains a large amount of water and alcohols; thus it is a prerequisite to separate water to produce fuel-grade biofuel. The separation alone was estimated to be 60-80% of total product cost.<sup>3</sup> Therefore, economical biofuel purification is indispensable.

Conventionally, the separation of alcohol/water is performed by distillation, which however is an energy intensive process.<sup>4</sup> Adsorption in porous materials is a technically feasible and economically attractive approach, and a wide range of materials such as activated carbons, polymeric resins, zeolites and their derivatives have been tested for the separation of alcohol/water.<sup>5,6</sup> Nevertheless, the adsorption capacity and/or selectivity in these adsorbents are not satisfactory and an ideal adsorbent should possess large surface area and pore volume, as well as high capacity and selectivity.

In the last decade, metal-organic frameworks (MOFs) have emerged as a new class of porous materials.<sup>7</sup> MOFs can be synthesized from various inorganic clusters and organic linkers, thus possess a wide range of surface area and pore size.<sup>7</sup> Consequently, MOFs have been considered as versatile materials potentially for separation, storage, catalysis and other applications.<sup>8</sup> Currently, most studies for MOFs have been focused on gas storage and separation, particularly the storage of low-carbon footprint energy carriers (e.g. H<sub>2</sub> and CH<sub>4</sub>) and the separation of CO<sub>2</sub>-containing gas mixtures for CO<sub>2</sub> capture.<sup>9-15</sup> Only very few experimental and simulation studies were conducted using MOFs for the separation of alcohol/water. Denayer and coworkers reported the liquid-phase adsorption isotherms of

alcohol/water mixtures in ZIF-8, and demonstrated that ZIF-8 has the largest uptake of butanol compared to active carbon and silicalite.<sup>16</sup> Chance and coworkers measured the adsorption of C<sub>1</sub> – C<sub>4</sub> alcohols and water in ZIF-8, ZIF-71, and ZIF-90, and further predicted the selectivity of alcohol/water.<sup>17,18</sup> Using simulation, we investigated the separation of ethanol/water mixtures in two MOFs, namely hydrophilic Na-*rho*-ZMOF and hydrophobic Zn<sub>4</sub>O(bdc)(bpz)<sub>2</sub>. The permselectivities were found to be primarily governed by adsorption rather than diffusion. This first simulation study on biofuel purification in MOFs provides bottom-up guidelines in the selection of appropriate MOFs.<sup>19</sup> Calero and coworkers simulated the separation of ethanol/water in Cu-BTC and proposed to selectively block and screen active sites to enhance separation factor.<sup>20</sup>

To develop novel MOFs for high-efficacy biofuel purification, it is crucial to quantitatively understand how purification performance is affected by tuning MOF structure and functionality. This is important, as pointed out above, unlimited number of MOFs could be synthesized and there exists a very large degree of freedom to improve performance. For CO<sub>2</sub> capture, a handful of strategies have been proposed to increase CO<sub>2</sub> capacity and selectivity such as tuning pore size/shape, exposing metal sites, functionalizing organic linkers.<sup>21,22</sup> In particular, functionalization is a commonly adopted approach as demonstrated by both experimental and simulation studies for CO<sub>2</sub> capture. For example, highly selective CO<sub>2</sub> uptake was observed in zeolitic imidazolate frameworks (ZIFs) possessing polar functionalities.<sup>23-26</sup> Separation of CO<sub>2</sub>/CH<sub>4</sub> and CO<sub>2</sub>/N<sub>2</sub> in UiO-66 was found to be tailored by various functional groups.<sup>27,28</sup> Post-combustion CO<sub>2</sub> capture in functionalized MIL-101 was predicted to be improved in terms of CO<sub>2</sub> capacity, CO<sub>2</sub>/N<sub>2</sub> selectivity, breakthrough time, and working capacity.<sup>29</sup> However, it is unknown how biofuel purification in MOFs would be affected by functionalization, as there has not been any study reported on this topic.

In this study, we aim to investigate biofuel purification in a series of ZIFs (ZIF-8, -90, -25, -71, -96 and -97) using molecular simulation. As a subset of MOFs, ZIFs have structural topologies similar to zeolites, in which the tetrahedral Si/Al nodes and O bridges are replaced by metal ions and imidazolate linkers, respectively. ZIFs possess exceptional chemical and thermal stability, in addition, the pore size and affinity of ZIFs are readily tunable. The six ZIFs simulated share the same metal clusters, but differ in imidazolate linkers with various functional groups. Therefore, the role of functional groups in biofuel purification will be elucidated from bottom-up, which could facilitate the development of new ZIFs and MOFs to improve biofuel purification. Following this introduction, the molecular models and simulation methods are described in Section 2. Similar to our previous study,<sup>19</sup> biofuel is represented by ethanol/water mixtures. In Section 3, the adsorption properties of pure ethanol and water in the six ZIFs are first presented and compared with available experimental data, and then the separation of ethanol/water mixtures is discussed. Finally, the concluding remarks are summarized in Section 4.

## 2. Models and methods

### 2.1. ZIFs and adsorbates

Fig. 1 illustrates the atomic structures of ZIF-8, -90, -25, -71, -96 and -97. They consist of the same tetrahedral  $ZnN_4$  clusters but different imidazolate linkers. Specifically, the linkers in ZIF-8, -90, -25, -71, -96 and -97 are 2-methyl imidazolate (meIm), imidazole-2-carboxyaldehyde imidazolate (icaIm), dimethyl imidazolate (dmeIm), dichloro imidazolate (dcIm), cyanideamine imidazolate (cyamIm), and hydroxymethylmethyl imidazolate (hymeIm), respectively. Among the six ZIFs, ZIF-8 and ZIF-90 possess the SOD type topology in which the linker is singly functionalized at position 2,<sup>30,31</sup> 4 and 6-membered rings are connected to form sodalite cages. In contrast, ZIF-25, -71, -96 and -97 belong to

RHO type with the linker dually functionalized at positions 4 and 5;<sup>24,32</sup> 4, 6 and 8-membered rings are connected to form truncated cuboctahedra ( $\alpha$ -cages) in a cubic body-centred arrangement.

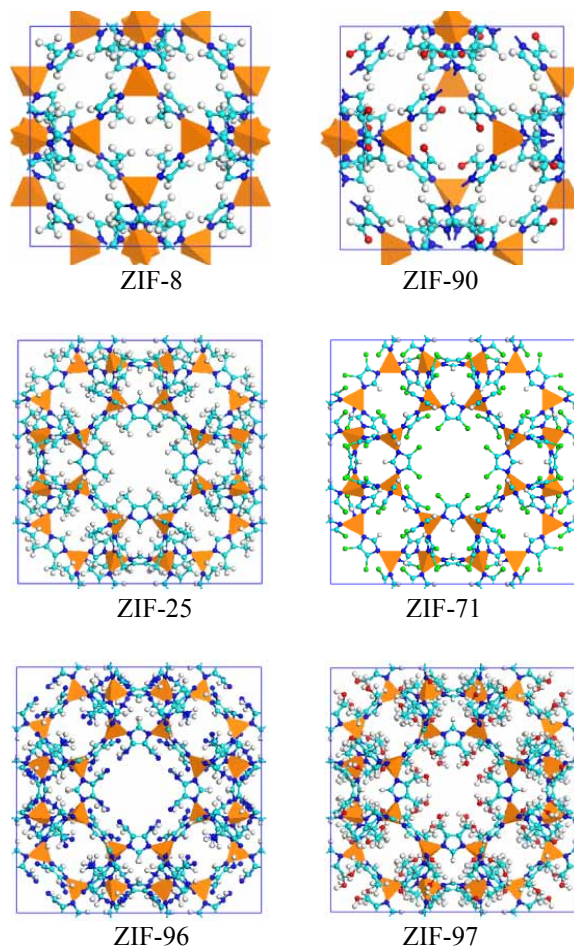


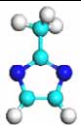
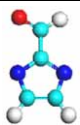
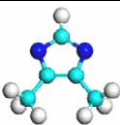



Fig. 1 Atomic structures of ZIF-8, -90, -25, -71, -96 and -97. ZnN<sub>4</sub> cluster: orange polyhedron, C: cyan, O: red, N: blue, Cl: green, and H: white. The size is not in the same scale.

In each ZIF, the accessible surface area, free volume, porosity, and pore size were calculated. Specifically, N<sub>2</sub> with a kinetic diameter of 3.64 Å was used as a probe to estimate the accessible surface area  $S_a$  by rolling the probe over framework surface.<sup>33</sup> Free volume  $V_f$  was estimated by randomly inserting He, a non-adsorbing species, into framework.<sup>34</sup> The ratio of free volume over framework volume gave porosity  $\phi$ . Pore size was calculated from the HOLE program,<sup>35</sup> including the diameter of cage ( $d_c$ ) and of aperture ( $d_a$ ). As illustrated



in Fig. S1 (ESI), the pore along the (111) direction in each ZIF is composed of alternating cage and aperture. Table 1 summarizes the structural properties of ZIF-8, -90, -25, -71, -96 and -97. The simulated surface areas agree fairly well with experimental BET values except for ZIF-8 and -97, plausibly due to the existence of solvent in experimental samples. Compared to ZIF-8 and ZIF-90, ZIF-25, -71, -96 and -97 generally possess smaller surface area  $S_a$  and free volume  $V_f$ , but larger cage  $d_c$ . The aperture diameter  $d_a$  in the six ZIFs ranges from 3.1 to 3.8 Å. In principle, a guest molecule with size larger than  $d_a$  cannot enter into the framework. However, it has been experimentally demonstrated that ZIF structures are not completely rigid and their aperture sizes can fluctuate, thus allow larger molecules to enter. For instance, several molecules (Ar, O<sub>2</sub>, N<sub>2</sub>, CH<sub>4</sub>, C<sub>2</sub>H<sub>6</sub>, C<sub>3</sub>H<sub>8</sub> and C<sub>4</sub>H<sub>10</sub>)<sup>23,30,36,37</sup> as well as ethanol, butanol, hexane, and xylene isomers<sup>38</sup> with kinetic diameter > 3.1 Å were found to adsorb and diffuse in ZIF-8.

Table 1. Structural Properties of ZIF-8, -90, -25, -71, -96 and -97.

	ZIF-8	ZIF-90	ZIF-25	ZIF-71	ZIF-96	ZIF-97
Linker						
	melm	icalm	dmelm	dcIm	cyamIm	hymelM
Topology	SOD	SOD	RHO	RHO	RHO	RHO
Space group	<i>I43m</i>	<i>I43m</i>	<i>Fd-3m</i>	<i>Pm-3m</i>	<i>I432</i>	<i>I432</i>
$a = b = c$ (Å)	16.9910 <sup>30</sup>	17.2715 <sup>31</sup>	28.6885 <sup>24</sup>	28.5539 <sup>32</sup>	28.5291 <sup>24</sup>	28.6011 <sup>24</sup>
$\rho$ (g/cm <sup>3</sup> ) <sup>a</sup>	0.924	0.988	0.949	1.155	0.977	0.997
	1279	1216	1029	1023	1128	835
$S_a$ (m <sup>2</sup> /g) <sup>b</sup>	(1630), <sup>30</sup> (1696) <sup>17</sup>	(1270), <sup>31</sup> (1280) <sup>17</sup>	(1110) <sup>24</sup>	(652), <sup>24</sup> (1183) <sup>17</sup>	(960) <sup>24</sup>	(564) <sup>24</sup>
$V_f$ (cm <sup>3</sup> /g)	0.531	0.480	0.443	0.447	0.518	0.400
$\phi$	0.491	0.474	0.420	0.516	0.506	0.399
$d_c$ (Å)	11.1	10.4	16.2	16.4	16.2	15.8
$d_a$ (Å)	3.1	3.5	3.3	3.5	3.8	3.3

<sup>a</sup>The densities are based on solvent-free perfect crystals. <sup>b</sup>Experimental BET surface areas are in parentheses.

The framework atoms of ZIFs were represented by Lennard-Jones (LJ) and Coulombic potentials



$$U_{\text{nonbonded}} = \sum 4\varepsilon_{ij} \left[ \left( \frac{\sigma_{ij}}{r_{ij}} \right)^{12} - \left( \frac{\sigma_{ij}}{r_{ij}} \right)^6 \right] + \sum \frac{q_i q_j}{4\pi\varepsilon_0 r_{ij}} \quad (1)$$

where  $\varepsilon_{ij}$  and  $\sigma_{ij}$  are the well depth and collision diameter,  $r_{ij}$  is the distance between atoms  $i$  and  $j$ ,  $q_i$  is the atomic charge of atom  $i$ ,  $\varepsilon_0 = 8.8542 \times 10^{-12} \text{ C}^2\text{N}^{-1}\text{m}^{-2}$  is the permittivity of vacuum. The atomic charges of ZIFs were calculated by the density functional theory (DFT) based on fragmental clusters as illustrated in Fig. S2 (ESI). The DFT calculations used the Becke exchange plus the Lee-Yang-Parr functional (B3LYP) and were carried out by Gaussian 03.<sup>39</sup> The accuracy of DFT-derived atomic charges depends on the choice of functional as well as basis set. Expressed as both local and gradient electron densities, the B3LYP has been widely used for solid materials. For small basis sets, the atomic charges fluctuate appreciably but tend to converge beyond 6-31G(d) basis set.<sup>40</sup> Therefore, 6-31G(d) was used for all the atoms of ZIFs except Zn atoms, for which the LANL2DZ basis set was used. By fitting the electrostatic potentials, the atomic charges were estimated as listed in Table S1 (ESI). In the literature, universal force field (UFF) and DREIDING force fields are widely used to mimic the LJ potentials of MOFs.<sup>34,41-43</sup> It is well recognized, however, these force fields overestimate the adsorption of small gas molecule (e.g. CO<sub>2</sub>, N<sub>2</sub>, and CH<sub>4</sub>) in ZIFs.<sup>44-46</sup> In our previous study, three different force fields including UFF, DREIDING, and AMBER were tested for the adsorption of C<sub>1</sub>-C<sub>4</sub> alcohols in ZIF-8; and DREIDING was found to exhibit the best agreement with experiment.<sup>47</sup> Hence, DREIDING is used in this study for the six ZIFs and the corresponding parameters are listed in Table S2 (ESI).

Ethanol was represented by a united-atom model with each CH<sub>x</sub> as a single interaction site. The potential parameters were adopted from the transferable potentials for phase equilibria (TraPPE) force field, which was fitted to measured critical properties and equilibrium data.<sup>48</sup> The bond lengths of ethanol were fixed, while the bending and torsional potentials were described by

$$U_{\text{bending}} = \sum \frac{1}{2} k_{\theta} (\theta_{ijk} - \theta_{ijk}^0)^2 \quad (2)$$

$$U_{\text{torsional}} = c_0 + c_1[1 + \cos \phi] + c_2[1 - \cos(2\phi)] + c_3[1 + \cos(3\phi)] \quad (3)$$

where  $k_{\theta}$  is force constant,  $\theta_{ijk}$  is bond angle and  $\theta_{ijk}^0$  is equilibrium angle;  $\phi$  is torsional angle and  $c_0/k_B = 0$ ,  $c_1/k_B = 209.82$ ,  $c_2/k_B = -29.17$  and  $c_3/k_B = 187.93$ . Water was mimicked by the three-point transferable interaction potential model (TIP3P).<sup>49</sup> The TIP3P gives reasonably good interaction energy compared to experiment. Table S3 (ESI) gives the potential parameters of ethanol and water. The cross interaction parameters were estimated by the Lorentz-Berthelot combining rules.

## 2.2. Simulation methods

To simulate the adsorption of pure ethanol and water as well as their mixtures, grand canonical Monte Carlo (GCMC) method was used. The chemical potentials of an adsorbate in adsorbed and bulk phases are identical at thermodynamic equilibrium, and GCMC method allows one to directly relate the chemical potentials in both phases and has been widely used to simulate adsorption.<sup>50,51</sup> For pure water and ethanol, the adsorption was simulated below saturation pressure, thus they were considered as ideal gases. The simulation box contained eight ( $2 \times 2 \times 2$ ) unit cells for ZIF-8 and ZIF-90, while one unit cell for ZIF-25, -71, -96 and -97, respectively. The periodic boundary conditions were exerted in all the three dimensions. It has been revealed that structural flexibility has a negligible effect on alcohol adsorption in ZIFs,<sup>47,52</sup> thus the ZIF structures were assumed to be rigid. In addition, possible inaccessible cages in the ZIFs were analysed using ethanol as a probe (4.46 Å in diameter). As illustrated in Fig. S3 (ESI), the 4-membered rings in ZIF-96 and ZIF-97 are inaccessible to ethanol, thus were blocked for ethanol adsorption during GCMC simulations. As demonstrated in our recent study, it is crucial to block inaccessible cages in GCMC simulations to avoid unrealistic adsorption.<sup>53</sup>

In the GCMC simulations, the LJ interactions were evaluated with a spherical cut-off of 15 Å. For the Coulombic interactions, the Ewald sum with a tin-foil boundary condition was used. The real/reciprocal space partition parameter and the cut-off for reciprocal lattice vectors were chosen to be  $0.2 \text{ \AA}^{-1}$  and 8, respectively, to ensure the convergence of the Ewald sum. The number of trial moves in a typical GCMC simulation was  $2 \times 10^7$ , in which the first half were used for equilibration and the second half for ensemble averages. Five types of trial moves were randomly attempted, namely displacement, rotation, partial regrowth at a neighbouring position, complete regrowth at a new position, and swap between reservoir including creation and deletion with equal probability. To improve sampling efficiency, configurational-bias technique was adopted in which an adsorbate molecule was grown atom-by-atom biasing towards energetically favourable configurations while avoiding overlap with other atoms.<sup>54-56</sup> Specifically, the trial positions were generated with a probability proportional to  $\exp(-\beta U_{\text{intra}}^i)$ , where  $\beta = 1/k_B T$  and  $U_{\text{intra}}^i$  is the intramolecular interaction energy at a position  $i$ . The numbers of trial positions for the first and subsequent atoms were fifteen and ten for pure ethanol and water, while twenty and fifteen for ethanol/water mixtures. One of the trial positions was then chosen with a probability proportional to  $\exp(-\beta U_{\text{inter}}^i) / \sum_i \exp(-\beta U_{\text{inter}}^i)$ , where  $U_{\text{inter}}^i$  is the intermolecular interaction energy. A modified version of BIGMAC code<sup>57</sup> was used for the GCMC simulations.

Furthermore, molecular dynamics (MD) simulations were conducted using GROMACS v.4.5.3<sup>58</sup> to estimate hydrogen-bonds (H-bonds). A hydrogen bond was assumed to form if the geometrical distance of donor and acceptor  $< 3.5 \text{ \AA}$  and the angle of acceptor – donor – hydrogen  $< 30^\circ$ . The initial configurations for the MD simulations were taken from the final configurations of GCMC simulations. Similarly, the ZIF structures were also treated to be rigid in the MD simulations. The Nosé-Hoover method was used to maintain the temperature

with a relaxation time of 0.1 ps. To calculate the Coulombic interactions, particle-mesh-Ewald technique was applied with a grid spacing of 0.12 and a fourth-order interpolation. The bond lengths of ethanol and water molecules were constrained using a linear constraint solver.<sup>59</sup> Each MD simulation was conducted for 12 ns, wherein the first 2 ns was used for equilibration and subsequent 10 ns was used for production. The potential and kinetic energies were monitored to ensure equilibration. The trajectory in production run was saved every 1 ps for analysis.

### 3. Results and discussion

First, the adsorption properties of pure ethanol in the six ZIFs are presented. From adsorption isotherms, hydrogen-bonds, isosteric heats, radial distribution functions, and density distribution contours, the role of functional groups is quantitatively assessed. Then, the adsorption of pure water is discussed, from which the hydrophobicity/hydrophilicity of the six ZIFs is classified. Finally, the separation of ethanol/water mixtures is examined and the highest selectivity is identified.

#### 3.1. Pure ethanol

Fig. 2 shows the adsorption isotherms of ethanol (EtOH) in ZIF-8, -90 and -71 at 308 K (35 °C). Fairly good agreement is observed between the simulated and experimental results in ZIF-8. Although the deviations in ZIF-90 and ZIF-71 are relatively large, the general feature of adsorption is captured by simulation. With increasing pressure, the isotherms can be characterized into three regions.<sup>47</sup> At low pressures, adsorption extent is small corresponding to cluster formation at preferential adsorption sites. With increasing pressure, cage-filling occurs with sharp increase in the uptake. Finally, saturation is gradually approached at high pressures. Apparently, the isotherms in ZIF-8 and ZIF-71 belong to *S*-shaped type V, which signifies the adsorption of weakly interacting adsorbate in a microporous structure. Similar

isotherms were observed in our previous simulation studies for alcohol adsorption in different MOFs.<sup>19,47,60,61</sup> Compared to ZIF-8 and ZIF-71, the isotherm in ZIF-90 is higher and its shape tends to become type I. This indicates that EtOH adsorption in ZIF-90 is stronger than in ZIF-8 and ZIF-71, as discussed below.

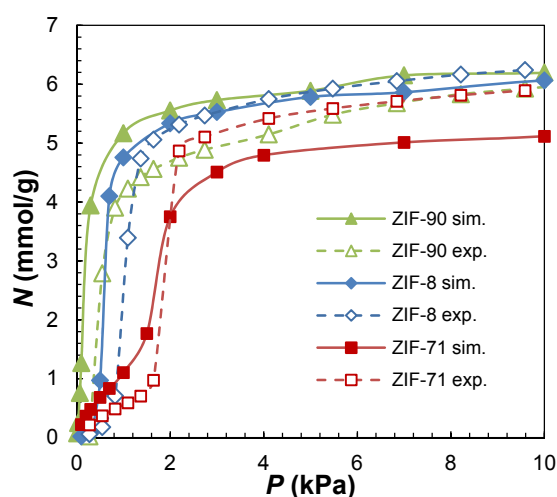


Fig. 2 Adsorption isotherms of EtOH in ZIF-8, -90 and -71 at 308 K. The experimental data are from ref. 17.

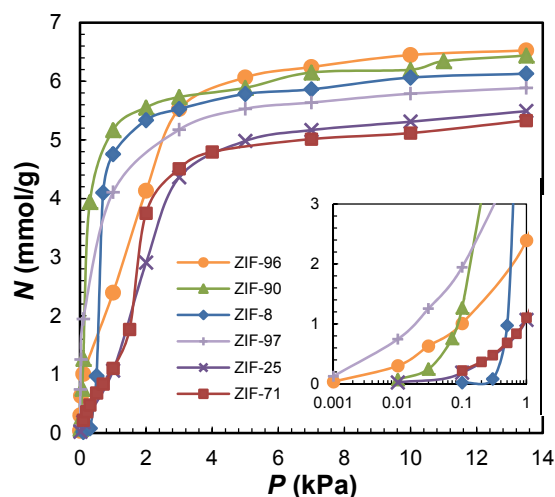


Fig. 3 Adsorption isotherms of EtOH in ZIF-8, -90, -25, -71, -96 and -97. The inset is the low-pressure region.

The simulated adsorption isotherms of EtOH in the six ZIFs are plotted in Fig. 3. In low-pressure region (e.g. 0.01 kPa), the uptake decreases in the order of ZIF-97 > -96 > -90 > -71

$\approx -25 > -8$ . Apparently, EtOH adsorption in ZIF-97, -96, and -90 is stronger than in ZIF-71, -25, and -8. This is because ZIF-97, -96 and -90 contain polar groups ( $-\text{CH}_2\text{OH}$ ,  $-\text{NH}_2$ ,  $-\text{CN}$  and  $-\text{COH}$ ) and can form hydrogen bonding (H-bonding) with EtOH. The strongest affinity in ZIF-97 is attributed to two factors: one is the capability to form H-bonding, and the other is the smallest free volume leading to the strongest overlap of surface potentials. In contrast, the groups ( $-\text{CH}_3$  and  $-\text{Cl}$ ) in ZIF-8, -25 and -71 are non- or weakly polar; therefore, no H-bonding is formed between framework and EtOH. Compared to ZIF-25 and ZIF-71, ZIF-8 exhibits the weakest affinity for EtOH. The reason is that ZIF-25 and ZIF-71 consist of two groups, instead of one in ZIF-8, thus possess stronger van der Waals interactions with EtOH.

To better evaluate the effect of functional groups on adsorption in high-pressure region, Fig. S4 (ESI) shows the adsorption isotherms of EtOH in ZIF-25, -71, -96 and -97 based on the number of molecules in simulation box. In high-pressure region, the contribution of porosity becomes increasingly important. This effect is observed among the four RHO-type ZIFs, in which ZIF-71 and ZIF-96 have a larger porosity than ZIF-25 and ZIF-97, and hence a greater uptake near saturation. Nevertheless, H-bonding also comes into play with porosity. For example, despite a smaller porosity compared to ZIF-71, ZIF-96 possesses a slightly greater saturation uptake because of H-bonding. This interplay also occurs between ZIF-25 and ZIF-97, i.e., ZIF-25 has a larger porosity but its saturation capacity is lower than ZIF-97.

Our previous study suggested that the effect of atomic charges is insignificant for alcohol adsorption in ZIF-8.<sup>47</sup> This effect is further examined here in all the six ZIFs. As shown in Fig. S5 (ESI), the adsorption isotherms of EtOH in symmetrically functionalized ZIF-8, -25, and -71 are only marginally affected by the inclusion of atomic charges. In asymmetrically functionalized ZIF-90, -96 and -97, however, the adsorption isotherms substantially decrease without atomic charges. This phenomenon, also observed for  $\text{CO}_2$  adsorption in several

ZIFs,<sup>24</sup> suggests that the Coulombic interaction in ZIFs is reduced by symmetrical functionalization.

As pointed out above, H-bonding has a significant effect on EtOH adsorption. Fig. 4 presents the number of hydrogen bonds (H-bonds). “ZIF-EtOH, EtOH-EtOH and total” refer to the H-bonds between ZIF and EtOH, EtOH and EtOH, and the sum of the two, respectively. The functional groups in ZIF-8, -25, and -71 are not polar, thus there are no ZIF-EtOH H-bonds. Nevertheless, the number of ZIF-EtOH H-bonds in ZIF-90, -96 and -97 increases with increasing amount of EtOH. It is interesting to note that ZIF-96 has the least number of H-bonds in these three ZIFs, suggesting that  $-\text{NH}_2$  and  $-\text{CN}$  groups in ZIF-96 have weaker capability to form H-bonding compared to  $-\text{COH}$  and  $-\text{CH}_2\text{OH}$  groups in ZIF-90 and ZIF-97. With regard to EtOH-EtOH H-bonds, the number increases in each ZIF when more EtOH is adsorbed. As a result, the total number of H-bonds also increases.

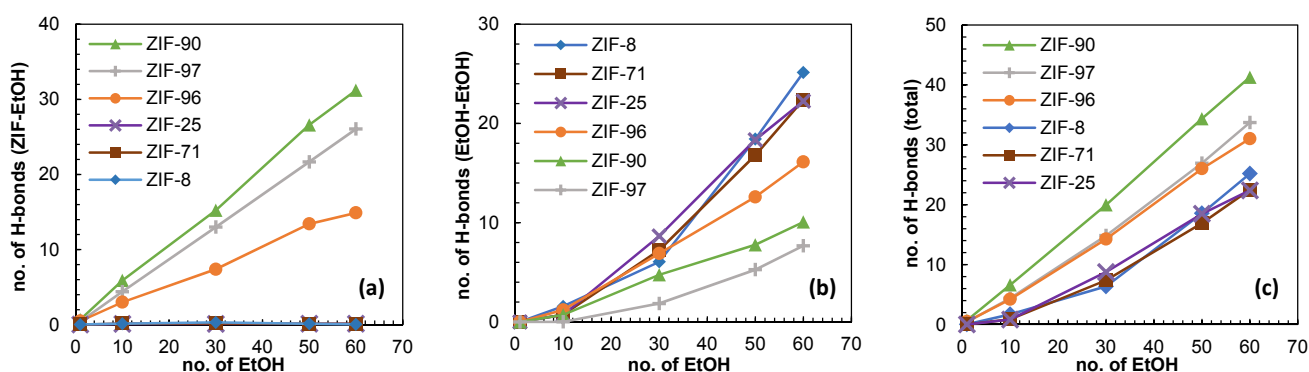


Fig. 4 Number of H-bonds (a) ZIF-EtOH (b) EtOH-EtOH and (c) total.

To quantitatively examine adsorption energy, the isosteric heat of adsorption was investigated as a function of loading. Specifically,  $Q_{\text{st}}^{\circ}$  at infinite dilution was estimated by a single-molecule MC simulation

$$Q_{\text{st}}^{\circ} = R_{\text{g}}T - U_{\text{ad}}^{\circ} \quad (4)$$

$$U_{\text{ad}}^{\circ} = U_{\text{total}} - (U_{\text{adsorbent}} + U_{\text{adsorbate}}) \quad (5)$$



where  $R_g$  is the gas constant,  $T$  is temperature,  $U_{\text{total}}$ ,  $U_{\text{adsorbent}}$  and  $U_{\text{adsorbate}}$  are the potential energies of adsorbent-adsorbate, adsorbent and a single adsorbate molecule, respectively. The conformational change of adsorbate upon adsorption was taken into account. At finite loadings,  $Q_{\text{st}}$  was estimated by

$$Q_{\text{st}} = R_g T - \left( \frac{\partial U_{\text{ad}}}{\partial N_{\text{ad}}} \right)_{T,V} \quad (6)$$

where  $U_{\text{ad}}$  and  $N_{\text{ad}}$  are adsorption energy and the number of adsorbate molecules, respectively. The partial derivative in the above equation was evaluated by

$$\left( \frac{\partial U_{\text{ad}}}{\partial N_{\text{ad}}} \right)_{T,V} = \frac{\langle N_{\text{ad}} U_{\text{ad}} \rangle - \langle N_{\text{ad}} \rangle \langle U_{\text{ad}} \rangle}{\langle N_{\text{ad}}^2 \rangle - \langle N_{\text{ad}} \rangle^2} \quad (7)$$

where the bracket  $\langle \dots \rangle$  denotes ensemble average.

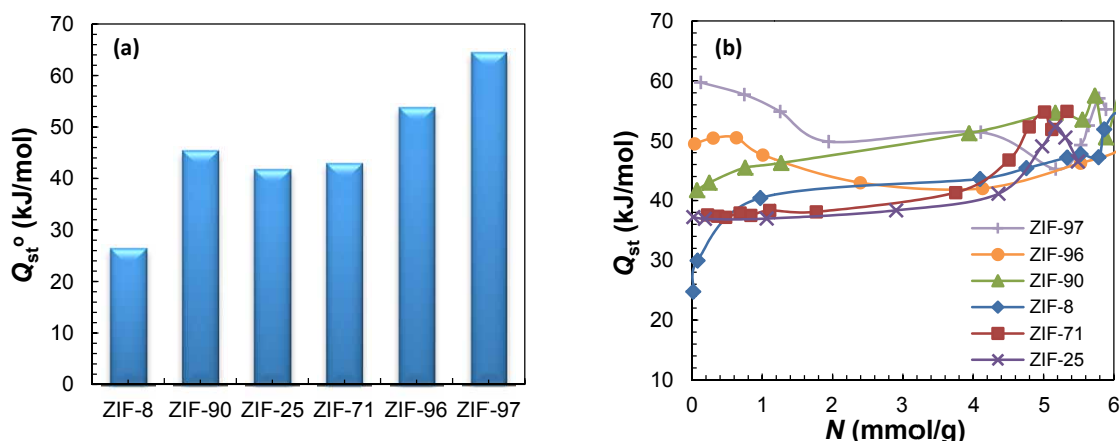


Fig. 5 Isothermic heats (a) infinite dilution and (b) finite loadings for EtOH adsorption in ZIF-8, -90, -25, -71, -96 and -97.

Fig. 5 shows the  $Q_{\text{st}}$  for EtOH adsorption in ZIF-8, -90, -25, -71, -96 and -97. For SOD-type ZIFs, ZIF-90 has a higher  $Q_{\text{st}}^{\circ}$  than ZIF-8 due to polar  $-\text{CHO}$  group. Similarly, for RHO-type ZIFs, ZIF-96 and ZIF-97 with polar  $-\text{NH}_2$ ,  $-\text{CN}$  and  $-\text{CH}_2\text{OH}$  groups exhibit higher  $Q_{\text{st}}^{\circ}$  than ZIF-25 and ZIF-71. Among the six ZIFs, ZIF-97 has the highest  $Q_{\text{st}}^{\circ}$ , followed by ZIF-

96, -90, -71, -25, and -8. This hierarchy is consistent with the uptake in low-pressure region (see Fig. 3). With increasing loading, interestingly,  $Q_{st}$  exhibits three trends in the six ZIFs. (1) In ZIF-8 and ZIF-90,  $Q_{st}$  monotonically increases as experimentally observed in ZIF-8.<sup>18</sup> The increase in ZIF-8 is particularly sharp at low loadings and attributed to the occurrence of H-bonding between EtOH molecules. Note that H-bonding cannot occur between EtOH and ZIF-8 due to the absence of donor or acceptor in ZIF-8. At intermediate loadings,  $Q_{st}$  in ZIF-8 and ZIF-90 increases slowly because EtOH molecules are dispersed in sodalite-cage and the EtOH-EtOH interaction is weak. At high loadings, EtOH molecules are closely packed and H-bonding is strong, leading to the further increase of  $Q_{st}$ . (2) In ZIF-25 and ZIF-71,  $Q_{st}$  marginally increases at low and intermediate loadings, and the magnitude of increase (or the slope) is less than in ZIF-8 and ZIF-90. The reason is that EtOH molecules are dispersed in  $\alpha$ -cage, which is larger than sodalite-cage, thus the EtOH-EtOH interaction in ZIF-25 and ZIF-71 is weaker compared to that in ZIF-8 and ZIF-90. At high loadings,  $Q_{st}$  distinctly increases as also seen in ZIF-8 and ZIF-90. (3) In ZIF-97 and ZIF-96,  $Q_{st}$  decreases (particularly in ZIF-97) at low and intermediate loadings because the favourable adsorption sites are gradually occupied as loading increases. Nevertheless,  $Q_{st}$  also increases at high loadings, as in the other four ZIFs, due to more compact packing.

It is instructive to characterize adsorption sites in the ZIFs. To do this, radial distribution functions for EtOH around the framework atoms were calculated by

$$g_{ij}(r) = \frac{N_{ij}(r, r + \Delta r)V}{4\pi r^2 \Delta r N_i N_j} \quad (8)$$

where  $r$  is the distance between atoms  $i$  and  $j$ ,  $N_{ij}(r, r + \Delta r)$  is the number of atom  $j$  around  $i$  within a shell from  $r$  to  $r + \Delta r$ ,  $V$  is the system volume,  $N_i$  and  $N_j$  are the numbers of atoms  $i$  and  $j$ , respectively. Fig. 6 shows the  $g(r)$  for EtOH around the heavy atoms (Zn, N, C and O) in the six ZIFs at 1 kPa. In ZIF-8, a peak at 5 Å exists in the  $g(r)$  around C2 atom, implying

the favourable location of EtOH proximal to the C=C bond of imidazolate linker. A lower peak at  $r = 4.5 \text{ \AA}$  is seen around C3 atom, thus  $-\text{CH}_3$  group is a less favourable site. The  $g(r)$  around Zn and C1 atoms only exhibit peaks at long distances (7 and  $6.2 \text{ \AA}$ ). This is consistent with methanol adsorption in ZIF-8 in our previous study.<sup>47</sup> In ZIF-90,  $-\text{CH}_3$  in ZIF-8 is replaced by  $-\text{CHO}$ . A sharp peak at  $2.9 \text{ \AA}$  is seen around O atom, which indicates strong interaction between  $-\text{CHO}$  and EtOH thus confirming the formation of H-bonding. In addition, C2 atom also acts as a favourable site at  $4.1 \text{ \AA}$ . For RHO-type ZIFs, ZIF-25 and ZIF-71 exhibit similar  $g(r)$ . A pronounced peak at  $4.9 \text{ \AA}$  exists in ZIF-25 and ZIF-71 around C3 and Cl atoms, respectively. This indicates  $-\text{CH}_3$  group in ZIF-25 and  $-\text{Cl}$  in ZIF-71 are the favourable sites. Furthermore, a lower peak is observed around C1 atom in both structures. In ZIF-96, the peaks at  $4.2 \text{ \AA}$  around N2, N3, and C4 atoms are almost equally significant. The reason is that  $-\text{NH}_2$  and  $-\text{CN}$  groups form H-bonding with EtOH, and thus the interactions are strong. In ZIF-97, a sharp peak around O atom implies strong interaction between  $-\text{CH}_2\text{OH}$  group and EtOH, again attributed to H-bonding. Moreover, peaks are also seen around C4 and C5 atoms, corresponding to  $-\text{CH}_3$  and  $-\text{CH}_2-$  groups. A common feature in the six ZIFs is that the peak around Zn atom is generally low at a long distance. Consequently, the imidazolate linkers are more favourable than the metal clusters in these ZIFs. This phenomenon is also observed in the experimental and simulation studies of gas adsorption in ZIFs.<sup>44-46,62-64</sup>

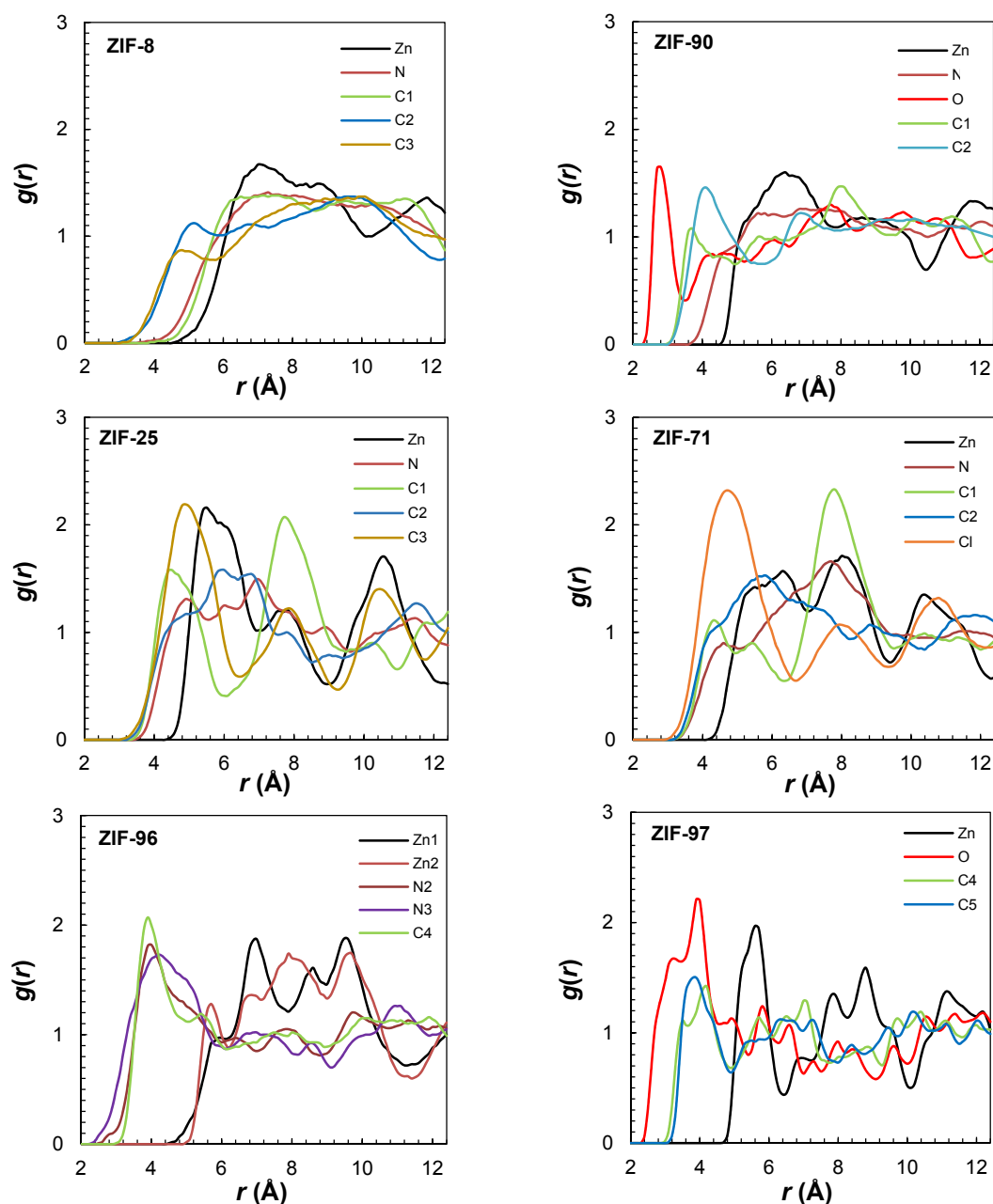


Fig. 6 Radial distribution functions for EtOH around the framework atoms of ZIF-8, -90, -25, -71, -96 and -97.

To visualize the locations of adsorbed EtOH molecules, Fig. 7 shows the density contours of EtOH in two ZIFs (ZIF-8 and ZIF-96). In ZIF-8, cluster is observed to form at a low pressure (0.1 kPa), proximally to the favourable site C=C bond at the aperture along the (111) direction. As pressure increases to 1 and 5 kPa, the density surrounding the less favourable site  $-\text{CH}_3$  group increases; meanwhile, cage-filling occurs in the sodalite cage. In ZIF-96, at

low and intermediate pressures (0.1 and 1 kPa), EtOH molecules are primarily populated near  $-\text{NH}_2$  and  $-\text{CN}$  groups at the aperture of  $\alpha$ -cage. At a high pressure (5 kPa), EtOH molecules are also located inside  $\alpha$ -cage and 6-membered ring.

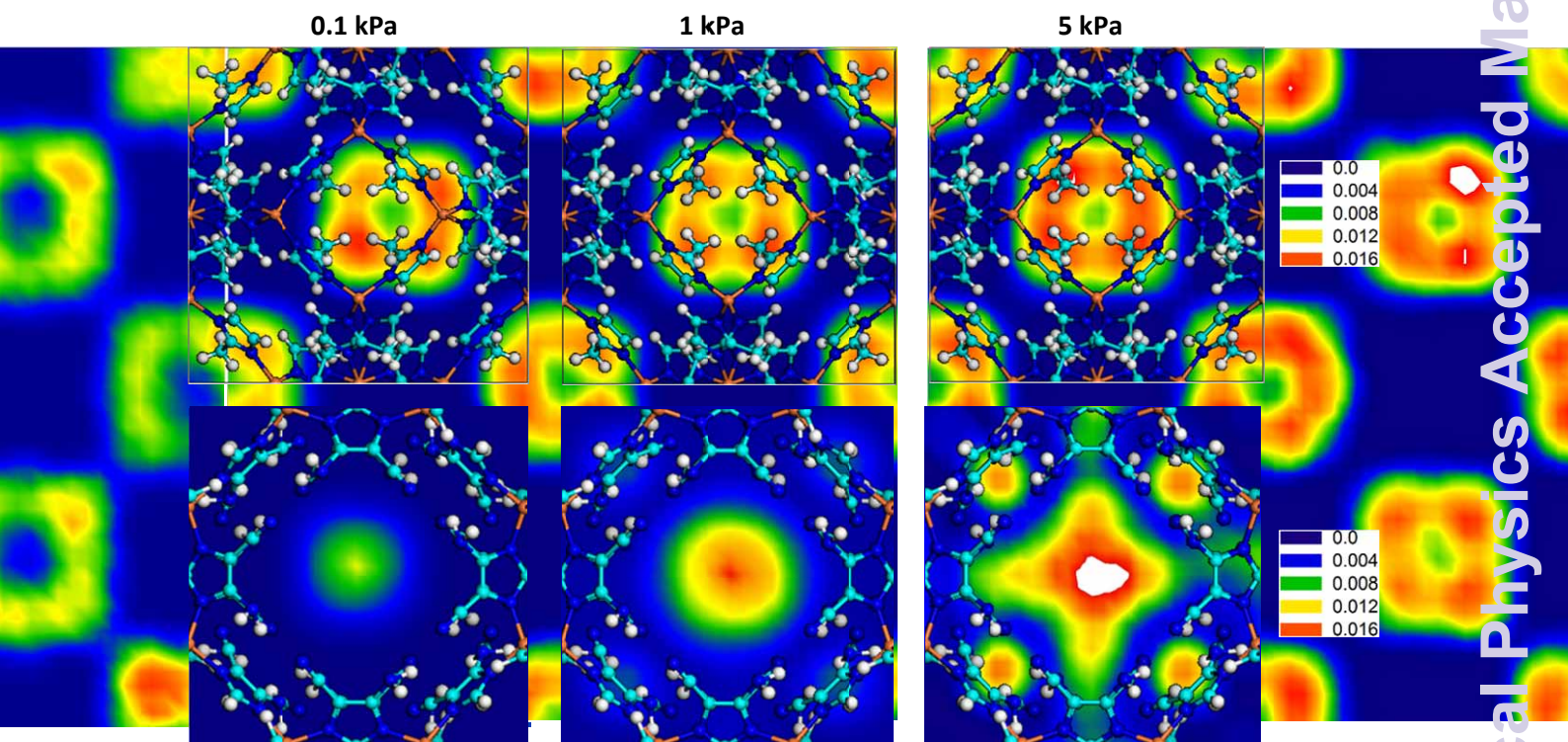


Fig. 7 Density contours of EtOH in ZIF-8 (top) and ZIF-96 (bottom). The unit of density scale is the number of molecules per  $\text{\AA}^3$ .

### 3.2. Pure water

Fig. 8a shows the adsorption isotherms of water ( $\text{H}_2\text{O}$ ) in ZIF-8, -71 and -90. The simulation results are in fairly good agreement with experimental data.<sup>17</sup>  $\text{H}_2\text{O}$  uptake in ZIF-8 and ZIF-71 is nearly zero, observed by both simulation and experiment. In ZIF-90,  $\text{H}_2\text{O}$  uptake is initially negligible but sharply increases beyond 1 kPa. Fig. 8b shows the adsorption isotherms in the six ZIFs. ZIF-8, -25 and -71 exhibit negligible adsorption below 5.58 kPa, the saturation pressure of  $\text{H}_2\text{O}$  (Table S4, ESI) and thus can be considered as *hydrophobic*. However, it is expected that capillary condensation would occur beyond the saturation pressure, as demonstrated previously in ZIF-71.<sup>60</sup> On the other hand, substantial adsorption is

observed in ZIF-90, -96, and -97, because they contain polar functional groups, can form H-bonding with H<sub>2</sub>O, and thus are *hydrophilic*. Such classification is in accord with the study by Amrouche et al.<sup>65</sup> Among the three hydrophilic ZIFs, ZIF-96 has the highest saturation capacity. As discussed above, this is because adsorption at high pressures is primarily governed by free volume; ZIF-96 possesses the largest free volume than ZIF-90 and ZIF-97, thus accommodating highest capacity.

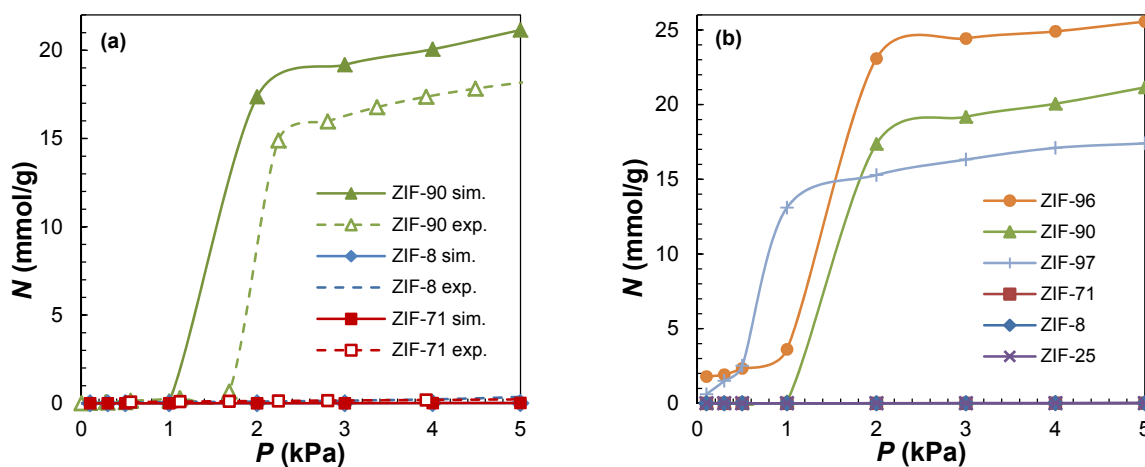


Fig. 8 Adsorption isotherms of H<sub>2</sub>O at 308 K in (a) ZIF-8, -71 and -90. The experimental data are from ref. 17. (b) ZIF-8, -71, -90, -25, -96 and -97.

Similar to EtOH, H-bonding also has a significant effect in H<sub>2</sub>O adsorption. Fig. 9 plots the number of H-bonds between ZIF and H<sub>2</sub>O, H<sub>2</sub>O and H<sub>2</sub>O, and the total, respectively. The functional groups in ZIF-90, -96, and -97 can form H-bonds with H<sub>2</sub>O, thus only these three ZIFs are examined. The number of ZIF-H<sub>2</sub>O H-bonds in ZIF-90, -96 and -97 increases with increasing amount of H<sub>2</sub>O adsorbed, and ZIF-96 has the largest number of H-bonds among the three ZIFs. This behaviour is different from EtOH in Fig. 4a, suggesting that H<sub>2</sub>O can form H-bonds more preferentially than EtOH in ZIF-96. As H<sub>2</sub>O has strong capability to form H-bonds and almost all H<sub>2</sub>O molecules adsorbed are involved in H-bonding. Consequently, the number of H<sub>2</sub>O-H<sub>2</sub>O H-bonds is much more compared to the number of



ZIF-H<sub>2</sub>O H-bonds. In the three ZIFs, the number of H<sub>2</sub>O-H<sub>2</sub>O H-bonds and the total number are close.

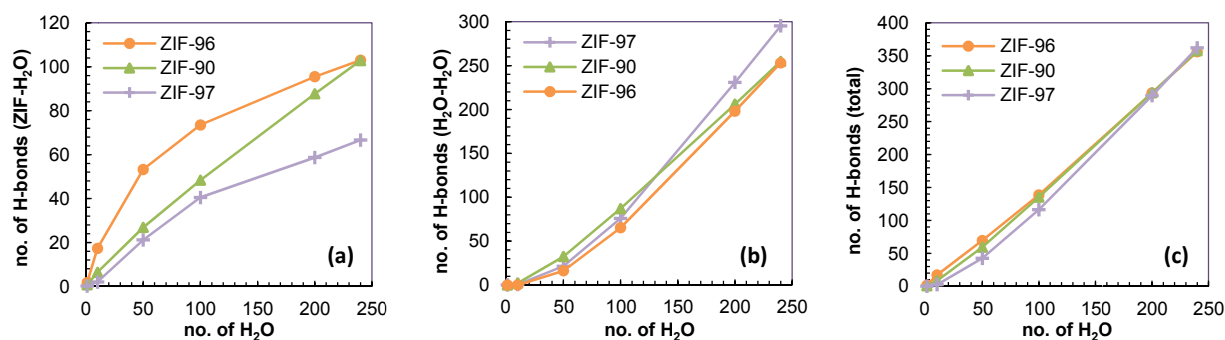


Fig. 9 Number of H-bonds (a) ZIF-H<sub>2</sub>O (b) H<sub>2</sub>O-H<sub>2</sub>O and (c) total.

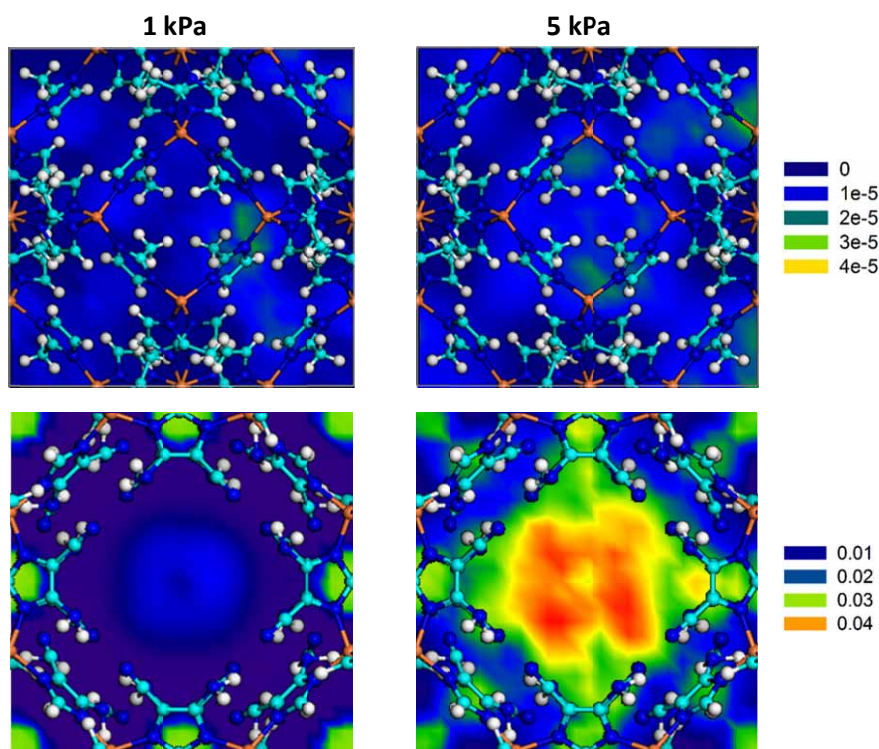


Fig. 10 Density contours of H<sub>2</sub>O in ZIF-8 (top) and ZIF-96 (bottom). The unit of density scale is the number of molecules per Å<sup>3</sup>.

Fig. 10 shows the density contours of H<sub>2</sub>O in ZIF-8 and ZIF-96 at 1 and 5 kPa, respectively. In ZIF-8, H<sub>2</sub>O has negligible adsorption at both pressures. This is because, as discussed above, ZIF-8 is hydrophobic and has very weak affinity for H<sub>2</sub>O. At 1 kPa, H<sub>2</sub>O



molecules in ZIF-96 are mainly located within the 4-membered ring due to strong potential overlap. With increasing pressure to 5 kPa, cage-filling occurs with the highest density at the cage centre, while the cage surface is also covered by H<sub>2</sub>O molecules.

### 3.3. Ethanol/water mixtures

Biofuel is mimicked by liquid mixtures of EtOH/H<sub>2</sub>O, in which the fugacity of component  $i$  is estimated by

$$f_i = P_i^{\text{sat}} \phi_i^{\text{sat}} X_i \gamma_i \exp\left(\frac{\bar{V}_i(P - P_i^{\text{sat}})}{RT}\right) \quad (9)$$

where  $P_i^{\text{sat}}$  is saturation pressure,  $\phi_i^{\text{sat}}$  is fugacity coefficient,  $X_i$  is mole fraction in liquid mixture,  $\gamma_i$  is activity coefficient,  $\bar{V}_i$  is partial molar volume,  $P$  and  $T$  are operating pressure and temperature. At the operating conditions considered in this study ( $P = 1$  bar and  $T = 298$  K),  $\phi_i^{\text{sat}}$  and the Poynting factor (the exponential term) are approximately equal to unity. The saturation pressures of EtOH and H<sub>2</sub>O were calculated by the Antoine equation (Table S4, ESI), and the activity coefficients (Fig. S6, ESI) were estimated by the Non-Random Two Liquid (NRTL) model.<sup>66</sup>

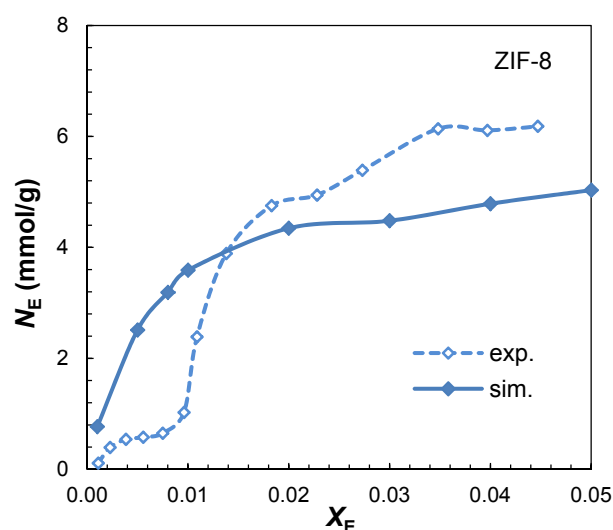


Fig. 11 EtOH uptake of EtOH/H<sub>2</sub>O mixtures in ZIF-8 at 298 K. The experimental data are from ref. 16.

Fig. 11 shows EtOH uptake of EtOH/H<sub>2</sub>O mixtures in ZIF-8 at 298 K. The experimental data by Denayer and coworkers<sup>16</sup> are also plotted. Compared to experiment, the simulated uptake is higher at  $X_E < 0.012$  and lower at  $X_E > 0.012$ . Nevertheless, the general trend is captured by simulation. The deviations between simulation and experiment are plausibly rooted in pure EtOH. As shown in Fig. 2, the simulated isotherm of EtOH in ZIF-8 agrees fairly well with experiment. From a closer look, however, we can see that simulation overestimates in low-pressure region, but underestimates in high-pressure region. Therefore, more accurate description is desired. Fig. S7 (ESI) shows the adsorption isotherms of EtOH/H<sub>2</sub>O mixtures in ZIF-8, -90, -25, -71, -96 and -97. With increasing  $X_E$ , EtOH uptake increases, whereas H<sub>2</sub>O uptake decreases in the six ZIFs. In hydrophobic ZIF-8, -25, and -71, although the uptake of pure H<sub>2</sub>O is negligible, H<sub>2</sub>O uptake from EtOH/H<sub>2</sub>O mixtures is enhanced because EtOH can act as seed for H<sub>2</sub>O adsorption.. This phenomenon was also observed in the adsorption of EtOH/H<sub>2</sub>O mixtures in highly hydrophobic Zn(bdc)(ted)<sub>0.5</sub>.<sup>61</sup>

To quantify the separation efficacy of EtOH/H<sub>2</sub>O mixtures, adsorption selectivity is defined by

$$S_{ad} = (Y_i/Y_j)/(X_i/X_j) \quad (10)$$

where  $Y_i$  and  $X_i$  are the compositions of component  $i$  in adsorbed and liquid phase, respectively. Fig. 12 shows the selectivities in ZIF-8, -90, -25, -71, -96 and -97 at 298 K. With increasing  $X_E$ , the selectivities monotonically drop. Similar trend was found by Chance and coworkers, who experimentally measured the isotherms of pure EtOH and H<sub>2</sub>O then theoretically predicted EtOH/H<sub>2</sub>O selectivities in ZIF-8, -71, and -90 using the ideal-adsorbed solution theory.<sup>17</sup> The magnitude of selectivities they predicted is close to the simulated values in this study. Normally, biofuel produced from biological feedstock contains dilute EtOH (< 5%). Among the six ZIFs, the selectivity in a dilute mixture (e.g.  $X_E = 5\%$ ) decreases following ZIF-8 > -71 ≥ -25 ≥ -90 > -97 > -96. The highest selectivity predicted in

ZIF-8 is approximately 32 at 1% of EtOH in the feed solution. We infer that hydrophobic ZIFs (ZIF-8, -71 and -25) possess higher selectivity compared to hydrophilic counterparts (ZIF-90, -97 and -96). The reason is that the polar groups in ZIF-90, -97 and -96 promote H<sub>2</sub>O adsorption and reduce EtOH/H<sub>2</sub>O selectivity. In the hydrophobic ZIFs (ZIF-8, -71 and -25), ZIF-8 exhibits the highest selectivity. This is because the sodalite cage in ZIF-8 is smaller than the  $\alpha$ -cage in ZIF-71 and ZIF-25, thus the separation performance is enhanced in ZIF-8. Similar enhancement was observed in the separation of alkane mixtures, in which catenated MOFs with restricted pores exhibit higher adsorption selectivity.<sup>67</sup>

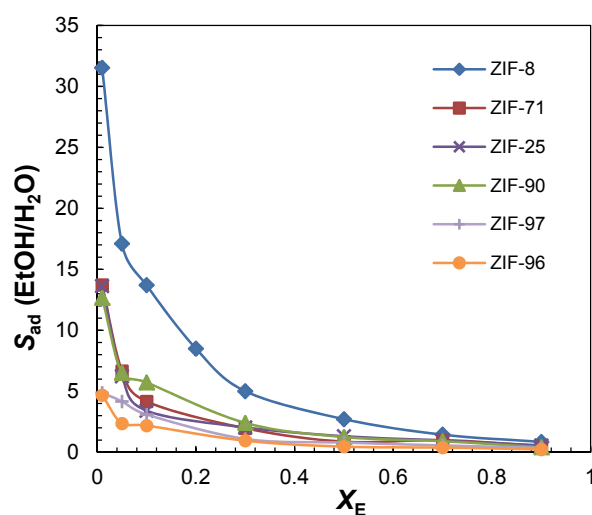


Fig. 12 Selectivity of EtOH/H<sub>2</sub>O mixtures in ZIF-8, -90, -25, -71, -96 and -97 at 298 K.

Fig. 13 shows the density contours of EtOH/H<sub>2</sub>O mixtures in two ZIFs (ZIF-8 with the highest selectivity and ZIF-96 with the lowest selectivity). At a low composition ( $X_E = 0.05$ ), EtOH in ZIF-8 is densely populated near the C=C bond of imidazolate linker and -CH<sub>3</sub> group, indicating the favourable interaction between EtOH and the linker in ZIF-8. Meanwhile, H<sub>2</sub>O is also strongly co-adsorbed. With increasing  $X_E$ , the density of EtOH increases slightly whereas H<sub>2</sub>O adsorption drops. In ZIF-96, H<sub>2</sub>O dominates the adsorption at a low  $X_E$ , with only a small amount of EtOH located in the cage centre. Even at  $X_E = 0.9$ , the functional

groups are primarily surrounded by H<sub>2</sub>O, while EtOH resides at the cage centre. This further confirms the low selectivity of EtOH over H<sub>2</sub>O in hydrophilic ZIF-96.

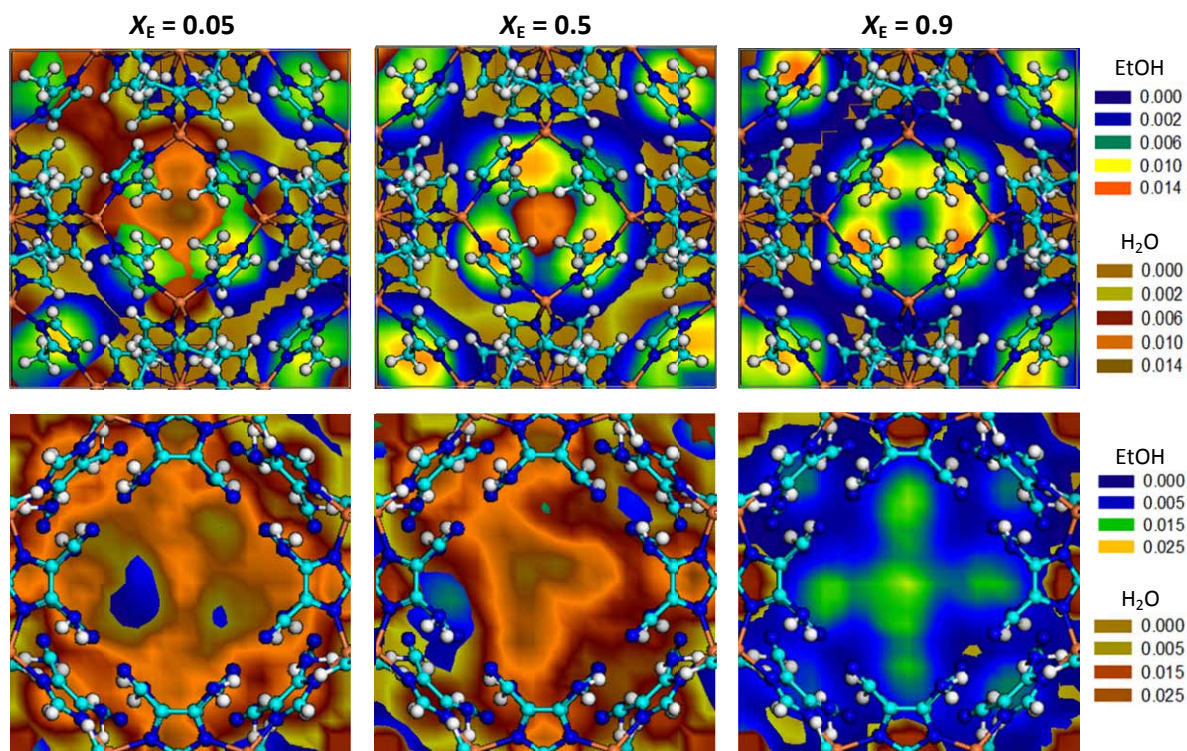


Fig. 13 Density contours of EtOH/H<sub>2</sub>O mixtures in ZIF-8 (top) and ZIF-96 (bottom). The unit of density scale is the number of molecules per Å<sup>3</sup>.

It is also intriguing to examine H-bonding during the adsorption of EtOH/H<sub>2</sub>O mixtures. Fig. 14 shows the number of H-bonds in ZIF-8 and ZIF-96. The number of H-bonds between ZIF-8 and adsorbate is zero over the whole range of  $X_E$ . As discussed above, no H-bond is formed between ZIF-8 and adsorbate. In hydrophilic ZIF-96, however, a larger number of H-bonds are formed with adsorbate, particularly H<sub>2</sub>O. It further reveals the polar functional groups in ZIF-96 interact more strongly with H<sub>2</sub>O compared to EtOH. Upon increasing  $X_E$ , the number of ZIF-EtOH H-bonds slightly rises, whereas the number of ZIF-H<sub>2</sub>O H-bonds substantially drops. Furthermore, the number of H-bonds per molecule drops in both ZIFs with increasing  $X_E$ . Interestingly, the number of H-bonds per molecule at  $X_E = 0.9$  in ZIF-96

is higher than that at  $X_E = 0.05$  in ZIF-8. This suggests that even at a very high  $X_E$ ,  $H_2O$  is still more preferentially adsorbed in ZIF-96 than in ZIF-8.

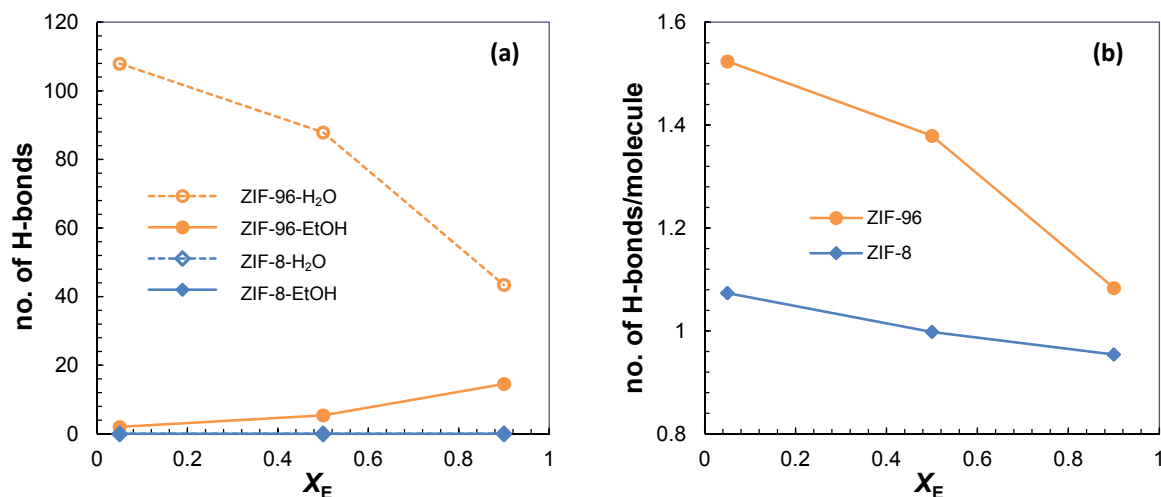


Fig. 14 (a) Number of ZIF-adsorbate H-bonds, (b) Number of H-bonds per adsorbate molecule.

#### 4. Conclusions

Adsorption and purification of biofuel in six ZIFs (ZIF-8, -25, -71, -90, -96 and -97) have been examined by molecular simulation. With polar functional groups, ZIF-97, -96 and -90 can form H-bonding with EtOH and  $H_2O$ . The number of H-bonds increases with increasing amount of adsorbate. In contrast, the functional groups in ZIF-8, -25 and -71 are non- or weakly polar, thus no H-bonding is formed. In low-pressure region, EtOH uptake decreases in the order of ZIF-97 > -96 > -90 > -71  $\approx$  -25 > -8. The isosteric heat of adsorption at infinite dilution follows the same order. As loading increases,  $Q_{st}$  exhibits three trends at low and intermediate loadings: monotonic increase in ZIF-8 and ZIF-90, marginal increase in ZIF-25 and ZIF-71, and decrease in ZIF-96 and ZIF-97. However,  $Q_{st}$  increases at high loadings in the six ZIFs. Furthermore, EtOH adsorption in ZIF-8, -25 and -71 with symmetric groups is not discernibly affected by the inclusion of atomic charges; however, the effect is substantial in ZIF-90, -96 and -97 with asymmetric groups. Hydrophobic ZIF-8, -25, and -71 exhibit

negligible adsorption of H<sub>2</sub>O, but substantial adsorption is observed in hydrophilic ZIF-90, -96 and -97. With regard to biofuel purification, the selectivity of EtOH over H<sub>2</sub>O drops as EtOH composition increases. This trend is consistent with theoretical prediction in the literature. Hydrophobic ZIF-8, -25 and -71 have higher selectivity than hydrophilic ZIF-90, -96 and -97. At a dilute mixture (e.g. 5% of EtOH), the selectivity decreases in the order of ZIF-8 > -71 ≥ -25 ≥ -90 > -97 > -96. ZIF-8 exhibits the highest selectivity and might be a potential candidate for biofuel purification.

### Acknowledgements

This work was supported by the National University of Singapore and the Ministry of Education of Singapore.

### References

- 1 J. Hill, E. Nelson, D. Tilman, S. Polasky and D. Tiffany, *Proc. Natl. Acad. Sci. U.S.A.*, 2006, **103**, 11206.
- 2 R. Luque, L. Herrero-Davila, J. M. Campelo, J. H. Clark, J. M. Hidalgo, D. Luna, J. M. Marinas and A. A. Romero, *Energy Environ. Sci.*, 2008, **1**, 542.
- 3 A. J. Ragauskas, C. K. Williams, B. H. Davison, G. Britovsek, J. Cairney, C. A. Eckert, W. J. Frederick, J. P. Hallett, D. J. Leak, C. L. Liotta, J. R. Mielenz, R. Murphy, R. Templer and T. Tschaplinski, *Science*, 2006, **311**, 484.
- 4 S. Venkatesan, Adsorption, in *Separation and Purification Technologies in Biorefineries* (John Wiley & Sons, Ltd, 2013), pp. 101.
- 5 R. K. Malik, P. Ghosh and T. K. Ghose, *Biotech. Bioeng.*, 1983, **25**, 2277.
- 6 R. A. Jones, F. H. Tezel, J. Thibault and J. S. Tolan, *Int. J. Energy Research*, 2007, **31**, 1517.



- 7 O. M. Yaghi, M. O'Keefe, N. W. Ockwig, H. K. Chae, M. Eddaoudi and J. Kim, *Nature*, 2003, **423**, 705.
- 8 G. Férey, *Chem. Soc. Rev.*, 2008, **37**, 191.
- 9 J. R. Li, R. J. Kuppler and H. C. Zhou, *Chem. Soc. Rev.*, 2009, **38**, 1477.
- 10 T. Düren, Y. S. Bae and R. Q. Snurr, *Chem. Soc. Rev.*, 2009, **38**, 1203.
- 11 D. H. Liu and C. L. Zhong, *J. Mater. Chem.*, 2010, **20**, 10308.
- 12 J. W. Jiang, R. Babarao and Z. Q. Hu, *Chem. Soc. Rev.*, 2011, **40**, 3599.
- 13 K. Sumida, D. L. Rogow, J. A. Mason, T. M. McDonald, E. D. Bloch, Z. R. Herm, T.-H. Bae and J. R. Long, *Chem. Rev.*, 2012, **112**, 724.
- 14 M. P. Suh, H. J. Park, T. K. Prasad and D. W. Lim, *Chem. Rev.*, 2012, **112**, 782.
- 15 R. B. Getman, Y. S. Bae, C. E. Wilmer and R. Q. Snurr, *Chem. Rev.*, 2012, **112**, 703.
- 16 J. Cousin Saint Remi, T. Rémy, V. Van Hunskerken, S. van de Perre, T. Duerinck, M. Maes, D. De Vos, E. Gobechiya, C. E. A. Kirschhock, G. V. Baron and J. F. M. Denayer, *ChemSusChem*, 2011, **4**, 1074.
- 17 K. Zhang, R. P. Lively, M. E. Dose, A. J. Brown, C. Zhang, J. Chung, S. Nair, W. J. Koros and R. R. Chance, *Chem. Commun.*, 2013, **49**, 3245.
- 18 K. Zhang, R. P. Lively, C. Zhang, W. J. Koros and R. R. Chance, *J. Phys. Chem. C*, 2013, **117**, 7214.
- 19 A. Nalaparaju, X. S. Zhao and J. W. Jiang, *Energy Environ. Sci.*, 2011, **4**, 2107.
- 20 J. J. Gutierrez-Sevillano, D. Dubbeldam, L. Bellarosa, N. Lopez, X. Liu, T. J. H. Vlugt and S. Calero, *J. Phys. Chem. C*, 2013, **117**, 20706.
- 21 J. W. Jiang, Metal-Organic Frameworks for CO<sub>2</sub> Capture: What are Learned from Molecular Simulations, in *Coordination Polymers and Metal Organic Frameworks*, edited by O. L. Ortiz and L. D. Ramírez (Nova Science Publishers, 2012).
- 22 J. W. Jiang, *Curr. Opin. Chem. Eng.*, 2012, **1**, 138.



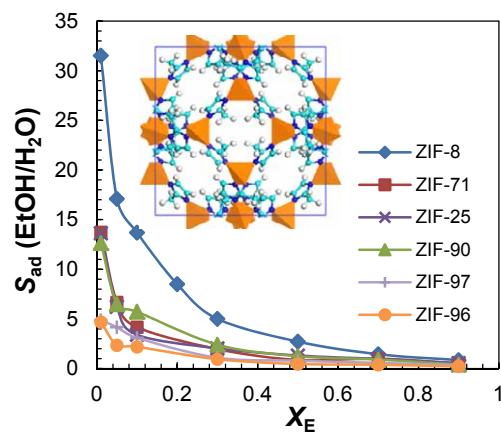
- 23 R. Banerjee, H. Furukawa, D. Britt, C. Knobler, M. O'Keeffe and O. M. Yaghi, *J. Am. Chem. Soc.*, 2009, **131**, 3875.
- 24 W. Morris, B. Leung, H. Furukawa, O. K. Yaghi, N. He, H. Hayashi, Y. Houndonougbo, M. Asta, B. B. Laird and O. M. Yaghi, *J. Am. Chem. Soc.*, 2010, **132**, 11006.
- 25 H. Amrouche, S. Aguado, J. Pérez-Pellitero, C. I. Chizallet, F. Siperstein, D. Farrusseng, N. Bats and C. Nieto-Draghi, *J. Phys. Chem. C*, 2011, **115**, 16425.
- 26 Y. A. Houndonougbo, C. Signer, N. He, W. Morris, H. Furukawa, K. G. Ray, D. L. Olmsted, M. D. Asta, B. B. Laird and O. M. Yaghi, *J. Phys. Chem. C*, 2013, **117**, 10326–10335.
- 27 Q. Y. Yang, A. D. Wiersum, P. L. Llewellyn, V. Guillermin, C. Serre and G. Maurin, *Chem. Commun.*, 2011, **47**, 9603.
- 28 G. E. Cmarik, M. Kim, S. M. Cohen and K. S. Walton, *Langmuir*, 2012, **28**, 15606.
- 29 K. Zhang, Y. F. Chen, A. Nalaparaju and J. W. Jiang, *CrystEngComm*, 2013, **15**, 10358.
- 30 K. S. Park, Z. Ni, A. P. Côté, J. Y. Choi, R. Huang, F. J. Uribe-Romo, H. K. Chae, M. O'Keeffe and O. M. Yaghi, *Proc. Nat. Acad. Sci.*, 2006, **103**, 10186.
- 31 W. Morris, C. J. Doonan, H. Furukawa, R. Banerjee and O. M. Yaghi, *J. Am. Chem. Soc.*, 2008, **130**, 12626.
- 32 R. Banerjee, A. Phan, B. Wang, C. Knobler, H. Furukawa, M. O'Keeffe and O. M. Yaghi, *Science*, 2008, **319**, 939.
- 33 T. Düren, F. Millange, G. Férey, K. S. Walton and R. Q. Snurr, *J. Phys. Chem. C*, 2007, **111**, 15350.
- 34 R. Babarao, Z. Q. Hu, J. W. Jiang, S. Chempath and S. I. Sandler, *Langmuir*, 2007, **23**, 659.
- 35 O. S. Smart, J. G. Neduvellil, X. Wang, B. A. Wallace and M. S. P. Sansom, *J. Mol. Graphics*, 1996, **14**, 354.

- 36 H. Bux, F. Liang, Y. Li, J. Cravillon, M. Wiebcke and J. Caro, *J. Am. Chem. Soc.*, 2009, **131**, 16000.
- 37 C. Zhang, R. P. Lively, K. Zhang, J. R. Johnson, O. Karvan and W. J. Koros, *J. Phys. Chem. Lett.*, 2012, **3** 2130.
- 38 K. Zhang, R. P. Lively, C. Zhang, R. R. Chance, W. J. Koros, D. S. Sholl and S. Nair, *J. Phys. Chem. Lett.*, 2013, **4**, 3618.
- 39 M. J. Frisch, G. W. Trucks, H. B. Schlegel, G. E. Scuseria, M. A. Robb, J. R. Cheeseman, V. G. Zakrzewski, J. A. Montgomery, R. E. Stratmann, J. C. Burant, S. Dapprich, J. M. Millam, A. D. Daniels, K. N. Kudin, M. C. Strain, O. Farkas, J. Tomasi, V. Barone, M. Cossi, R. Cammi, B. Mennucci, C. Pomelli, C. Adamo, S. Clifford, J. Ochterski, G. A. Petersson, P. Y. Ayala, Q. Cui, K. Morokuma, D. K. Malick, A. D. Rabuck, K. Raghavachari, J. B. Foresman, J. Cioslowski, J. V. Ortiz, B. B. Stefanov, G. Liu, A. Liashenko, P. Piskorz, I. Komaromi, R. Gomperts, R. L. Martin, D. J. Fox, T. Keith, M. A. Al-Laham, C. Y. Peng, A. Nanayakkara, C. Gonzalez, M. Challacombe, P. M. W. Gill, B. G. Johnson, W. Chen, M. W. Wong, J. L. Andres, M. Head-Gordon, E. S. Replogle and J. A. Pople, *Gaussian 03*, Revision D.01 ed. Gaussian Inc., Wallingford CT, 2004.
- 40 P. C. Hariharan and J. A. Pople, *Chem. Phys. Lett.*, 1972, **16**, 217.
- 41 G. Garberoglio, A. I. Skoulidas and J. K. Johnson, *J. Phys. Chem. B*, 2005, **109**, 13094.
- 42 A. I. Skoulidas and D. S. Sholl, *J. Phys. Chem. B*, 2005, **109**, 15760.
- 43 R. Babarao and J. W. Jiang, *Langmuir*, 2008, **24**, 6270.
- 44 J. Perez-Pellitero, H. Amrouche, F. R. Siperstein, G. Pirngruber, C. Nieto-Draghi, G. Chaplais, A. Simon-Masseron, D. Bazer-Bachi, D. Peralta and N. Bats, *Chem. Eur. J.*, 2010, **16**, 1560.
- 45 J. G. McDaniel, K. Yu and J. R. Schmidt, *J. Phys. Chem. C*, 2011, **115**, 10054.
- 46 D. Fairen-Jimenez, R. Galvelis, A. Torrissi, A. D. Gellan, M. T. Wharmby, P. A. Wright, C. Mellot-Draznieks and T. Düren, *Dalton Trans.*, 2012, **41**, 10752.

- 47 K. Zhang, L. Zhang and J. W. Jiang, *J. Phys. Chem. C*, 2013, **117**, 25628.
- 48 B. Chen, J. J. Potoff and J. I. Siepmann, *J. Phys. Chem. B*, 2001, **105**, 3093.
- 49 W. L. Jorgensen, J. Chandrasekhar, J. D. Madura, R. W. Impey and M. L. Klein, *J. Chem. Phys.*, 1983, **79**, 926.
- 50 M. P. Allen and D. J. Tildesley, *Computer Simulation of Liquids*. Oxford University Press, Oxford, 1987.
- 51 D. Frenkel and B. Smit, *Understanding Molecular Simulation: From Algorithms to Applications*. Academic Press, San Diego, 2002.
- 52 J. A. Gee, J. Chung, S. Nair and D. S. Sholl, *J. Phys. Chem. C*, 2013, **117**, 3169.
- 53 K. Zhang, A. Nalaparaju, Y. F. Chen and J. W. Jiang, *RSC Adv.*, 2013, **3**, 16152.
- 54 D. Frenkel, G. C. A. M. Mooij and B. Smit, *J. Phys.: Condensed Matter*, 1992, **4**, 3053.
- 55 J. J. de Pablo, M. Laso and U. W. Suter, *J. Chem. Phys.*, 1992, **96**, 2395.
- 56 J. I. Siepmann and D. Frenkel, *Mol. Phys.* 1992, **75**, 59.
- 57 T. J. H. Vlugt and B. Smit, <http://molsim.chem.uva.nl/bigmac>.
- 58 D. Van Der Spoel, E. Lindahl, B. Hess, G. Groenhof, A. E. Mark and H. J. C. Berendsen, *J. Comput. Chem.*, 2005, **26**, 1701.
- 59 B. Hess, H. Bekker, H. J. C. Berendsen and J. G. E. M. Fraaije, *J. Comput. Chem.*, 1997, **18**, 1463.
- 60 A. Nalaparaju, X. S. Zhao and J. W. Jiang, *J. Phys. Chem. C*, 2010, **114**, 11542.
- 61 Y. F. Chen, J. Y. Lee, R. Babarao, J. Li and J. W. Jiang, *J. Phys. Chem. C*, 2010, **114**, 6602.
- 62 H. Wu, W. Zhou and T. Yildirim, *J. Am. Chem. Soc.*, 2007, **129**, 5314.
- 63 H. Wu, W. Zhou and T. Yildirim, *J. Phys. Chem. C*, 2009, **113**, 3029.
- 64 L. L. Zhang, Z. Q. Hu and J. W. Jiang, *J. Am. Chem. Soc.*, 2013, **135**, 3722.

- 65 H. Amrouche, B. Creton, F. Siperstein and C. Nieto-Draghi, *RSC Advances*, 2012, **2**, 6028.
- 66 K. Kurihara, T. Minoura, K. Takeda and K. Kojima, *J. Chem. Eng. Data*, 1995, **40**, 679.
- 67 R. Babarao, Y. H. Tong and J. W. Jiang, *J. Phys. Chem. B*, 2009, **113**, 9129.

## Table of Contents Entry



Functional groups of zeolitic imidazolate frameworks play a significant role in the adsorption of ethanol and water, and biofuel purification.